Chemical Papers (2021) 75:2295–2304
https://doi.org/10.1007/s11696-020-01448-z

ORIGINAL PAPER

Morphology controlled synthesis of one-dimensional $CoMn_2O_4$ nanorods for high-performance supercapacitor electrode application

T. Antony Sandosh[1,2] · A. Simi[2]

Received: 27 July 2020 / Accepted: 22 November 2020 / Published online: 5 January 2021

Abstract

Facile preparation of one-dimensional spinel material is highly attractive for their widespread usage in energy storage devices. Herein, we report uniform one-dimensional $CoMn_2O_4$ nanorods were prepared by cetyl trimethyl ammonium bromide (CTAB) assisted hydrothermal technique followed by subsequent calcination process. The prepared materials were characterized to different types of physicochemical features to analyze the appropriateness of the material for the supercapacitor electrode application. The crystalline nature and bonding properties were examined by X-ray diffraction analysis and Fourier-transform infrared spectroscopic analysis. The structural and morphological features of prepared materials were analyzed using field emission scanning electron microcopy which reveals the edge curved one-dimensional nanorod structure. Furthermore, cyclic voltammetric, chronopotentiometric and electrochemical impedance spectroscopic analyses were employed to evaluate the electrochemical properties of the freshly prepared $CoMn_2O_4$ materials. The cyclicvoltammetric studies provide the specific capacitance of 895 Fg^{-1} at a scan rate of 5 mV s^{-1}, whereas chronopotentiometric curves provide the highest specific capacitance of 802 Fg^{-1} at current density of 1 Ag^{-1}. The cyclic stability analysis shows the excellent cyclic stability which retains 87% of initial capacitance after the continuous 5000 CV cycles at a scan rate of 100 mVs^{-1}. The outstanding electrochemical features unquestionably make $CoMn_2O_4$ as a good candidate for supercapacitor devices.

Keywords Spinel · CTAB · Hydrothermal · $CoMn_2O_4$ nanorods · Energy storage · Supercapacitors

Introduction

The rapid economic growth in recent decades has endorsed the alarming conflict between high requirement of fossil fuels and their restricted resources. To resolve this problem, researchers have been looking for efficient relevant technologies to fabricate renewable energy storage and conversion devices whereas conserving the surroundings(Zhu et al. 2015; Wang et al. 2016; Abbasi et al. 2020; Amiri et al. 2020; Moosavifard et al. 2020). Supercapacitors or electrochemical capacitors, as a new kind of energy storage device, have fascinated more consideration since their interesting characteristics such as high-power density than batteries and high energy density than conventional capacitors (Chen et al. 2014; Xu et al. 2014a, b). With a combination, consolidation of high power density and comparatively high energy density, supercapacitors have been generally utilized in various kinds of applications including memory backup systems, wireless networks, automotives, portable consumer electronics, motor starters and other self-powered micro/nano-electronics (Simon 2008; Zhu et al. 2008; Yesuraj et al. 2017). Supercapacitors can be categorized into two types such as electric double-layer capacitors (EDLC) and pseudocapacitors based on the energy storage mechanism (Zhang et al. 2017, 2019). In electric double-layer capacitors, the charge is stored by accumulation of charges at the electrode/electrolyte interface by achieving the formation of electric double layers (Makino et al. 2013; Wulan Septiani et al. 2020). Mostly, carbon-based materials (carbon nanotube, activated carbon, carbon aerogel and graphene oxide) exhibit the electric double layer energy storage mechanism. On the other hand, the pseudocapacitor materials such as metal oxides and conducting polymers can store charges

✉ T. Antony Sandosh
antonysandosh11@gmail.com

[1] Department of Chemistry, St. Joseph's College of Arts and Science (Autonomous), Affiliated to Thiruvalluvar University, Vellore, Cuddalore 607001, India

[2] Department of Chemistry, St. Joseph's College (Autonomous), Affiliated To Bharathidasan University, Tiruchirappalli 620002, India

through rapid and reversible surface redox reactions and it possesses much higher specific capacitance than electric double layer capacitor materials(Chen et al. 2013; Li et al. 2013; Wu et al. 2014). Therefore, developing of novel and proficient pseudocapacitor electrode materials with attractive electrochemical performances such as high electrical conductivity, electrochemical stability combined with novel structural features such as high surface area and porous structure is the hot research topic in recent years.

Transition metal oxides such as NiO (Yan et al. 2014), MnO_2(Boisset et al. 2013), Co_3O_4(Xia et al. 2011), MoO_3(Zhao et al. 2013), V_2O_5(Yang et al. 2013), SnO_2(Geng et al. 2020) and ZnO (Naeem et al. 2020) materials have been examined intensively as the advanced electrode materials for supercapacitor device application since they exhibit multiple oxidation states for fast redox reactions, low-cost and eco-friendly nature. In contrast, these aforementioned materials often experience the poor cycle life, limited rate capability and poor mechanical stability when used as supercapacitor electrode materials (An et al. 2019; Li et al. 2019; Low et al. 2019). Also, they exhibit relatively low capacitance when compared with RuO_2 (Hu et al. 2006) (identified as a potential supercapacitor electrode material) and these limitations have restricted their utilization in commercial supercapacitors. Consequently, it is a huge task to prepare electrode materials with superior electrochemical performances and fulfill the drawbacks of single transition metal oxide-based supercapacitor electrode materials.

Recently, mixed metal oxides such as $ZnCo_2O_4$(Mary and Bose 2018), $NiCo_2O_4$(Pu et al. 2013), $MnCo_2O_4$(Che et al. 2016), $CuCo_2O_4$(Vijayakumar et al. 2017) and $CoMn_2O_4$ are demonstrated as efficient electrode materials for supercapacitors because of their mixed valence states that afford higher electrochemical activity and superior electronic conductivity than single metal oxides. Among them, Mn-based materials are of great interest because of their high electrical conductivity, low-cost and easily abundance and eco-friendly nature. Spinel structured $CoMn_2O_4$ exhibits high electrical conductivity and attractive electrochemical features when compared with corresponding single metal oxides such as Co_3O_4 and Mn_3O_4 (Yunyun et al. 2015). By altering the surface morphological features, the electrochemical properties of the $CoMn_2O_4$ materials could be considerably enhanced. Recently, Ji and Zhou et al. prepared cubic $CoMn_2O_4$ particles which directly grown on Ni foam through hydrothermal method. The prepared $CoMn_2O_4$ particles were used as binder-free electrode which provides a capacity of 140.6 mA h g^{-1} at 1 mA cm^{-2} in three electrode configuration and an asymmetric device exhibits a specific capacitance of 77.8 Fg^{-1} at 2 mA cm^{-2} (Chen et al. 2019a, b). Potheher et al. demonstrated $CoMn_2O_4$ material synthesized through hydrothermal technique. This material possessed the specific capacitance of 700 Fg^{-1} at a scan rate of 5 mV s^{-1}(Vigneshwaran et al. 2016). Furthermore, Xuetang and Fan et al. established Spinel $CoMn_2O_4$ nanosheet arrays grown on Ni foam via hydrothermal route. The nanosheet arrays provide a specific capacitance of 1529 Fg^{-1} and good rate capability. The cyclic stability studies showed that the 100% stability after 3000 cycles (Yunyun et al. 2015). Wang et al. prepared both $MnCo_2O_4$ and $CoMn_2O_4$ nanowires using thermal decomposition of organometallic compounds. The $MnCo_2O_4$ and $CoMn_2O_4$ affords the specific capacitance of 2108 and 1342 Fg^{-1}, respectively, at a current density of 1 Ag^{-1}(Paquin et al. 2015). Consequently, it is important to take essential steps for enhancing the supercapacitive properties of the $CoMn_2O_4$ materials. The various synthetic routes are widely explored, including hydrothermal method, templates synthesis, co-precipitation method, thermal conversion, electrochemical deposition and many other methods. Among them, hydrothermal method has been recognized as a powerful method to provide size-controllable and well-ordered nanostructured morphology. In this endeavour, we followed the CTAB-assisted hydrothermal method to prepare $CoMn_2O_4$ materials (Dhand et al. 2015).

Herein, we report one-dimensional $CoMn_2O_4$ nanorods via CTAB-assisted hydrothermal technique followed by subsequent calcination process which also involved the variation of CTAB template concentration. Electrochemical measurements show that the prepared $CoMn_2O_4$ material had better supercapacitive features with a high specific capacitance of 895 Fg^{-1} at a scan rate of 5 mVs^{-1}. In addition, cyclic stability studies shows that the prepared $CoMn_2O_4$ material retained 92% of specific capacitance after 2000 cycles. The outstanding electrochemical features made as the freshly prepared $CoMn_2O_4$ nanorod as a promising material for supercapacitor electrode applications.

Experimental section

Materials

All chemical reagents were analytical grade and utilized as received. Cobalt(II) nitrate hexahydrate ($Co(NO_3)_2{\cdot}6H_2O$), poly (vinylidene fluoride) (PVDF), carbon black and cetyltrimethylammonium bromide (CTAB) were procured from Sigma Aldrich. N-methyl- 2-pyrrolidone (NMP), potassium hydroxide (KOH), Manganese nitrate tetrahydrate ($Mn(CH_3COO)_2.4H_2O$) and ethanol were purchased from SRL (India). In addition, acetone and nickel foil (0.025 mm thickness) were received from Alfa aesar.

Synthesis of $CoMn_2O_4$ materials

The CTAB-assisted hydrothermal synthetic method has been followed for the preparation of spinel $CoMn_2O_4$ materials. In a typical preparation of $CoMn_2O_4$ materials, 1 mM of cobalt nitrate hexahydrate and 2 mM of manganese nitrate tetrahydrate were dissolved in 70 ml of DI water at room temperature using magnetic stirrer with rotating speed of 450 rpm. Then, CTAB template was added to the above suspension and stirred for half an hour. After the complete dissolution of all precursors, the suspension was transferred to 100 ml of teflon lined stainless steel autoclave and kept in hot air oven. The hot air oven was heated to 180 °C for 24 h and then it is allowed to cool room temperature normally. The resultant precipitate was collected and washed with water and ethanol to remove impurities and unreacted species. Then, it is dried in a hot oven at 80 °C for 12 h and calcined in air at 300 °C for 3 h with ramping rate of 10 °C/min. In this endeavour, the CTAB concentration was varied to get the different type of nanostructure $CoMn_2O_4$ materials. The CTAB concentrations such as 0, 0.005, 0.01 and 0.02 M were used to prepare $CoMn_2O_4$-1, $CoMn_2O_4$-2, $CoMn_2O_4$-3 and $CoMn_2O_4$-4 samples, respectively. Figure 1 shows the schematic diagram of synthesis of $CoMn_2O_4$-4 material.

Material characterization

The X-ray diffraction (XRD) patterns were acquired on a PANalytical X-pert PRO diffractometer instrument with Ni filtered Cu-Kα radiation ($\lambda = 0.154060$ nm) at a voltage of 40 kV and a current of 40 mA. Fourier transform infrared spectroscopy (FTIR) was recorded using Perkin-Elmer RX1′ spectrophotometer instrument with 4 cm^{-1} resolution for 20 scans and field-emission scanning electron microscope (FE-SEM, Hitachi SU6600) operated with an accelerating voltage of 15 kV for obtained morphological features.

Electrochemical measurements

For electrochemical measurement, the working electrode comprising of 70 wt% of active material, 10 wt% of carbon black and 10 wt% of poly (vinylidene fluoride) (PVDF). For electrochemical analysis, the above-mentioned materials made slurry with N-methyl-2- pyrrolidone (NMP) solvent. The resultant slurry was coated uniformly on the surface (two side) of nickel foil and dried in hot air oven at 60 °C for 12 h. The active material's weight of the electrode is approximately 3 mg. The supercapacitor analysis was done on a biologic electrochemical workstation (Model VSP-150) in three electrode set up using 2 M KOH as an electrolyte. Standard calomel electrode and platinum foil were used as counter and reference electrodes, respectively. The supercapacitive properties of the $CoMn_2O_4$ material were examined by cyclic voltammetric (CV), chronopotentiometric (CP) or galvanostatic charge/discharge (GCD) and electrochemical impedance studies (EIS). Additionally, cyclic stability test was also carried out to demonstrate cycle life of the $CoMn_2O_4$ electrodes.

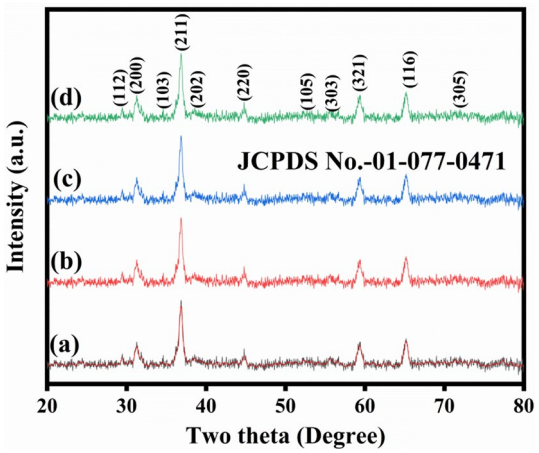

Fig. 2 XRD patterns of $CoMn_2O_4$ materials. **a** $CoMn_2O_4$-1, (**b**) $CoMn_2O_4$-2, (**c**) $CoMn_2O_4$-3 and (**d**) $CoMn_2O_4$-4

Results and discussion

X-ray diffraction analysis

The phase purity and crystallographic nature of the freshly prepared $CoMn_2O_4$ materials were examined by

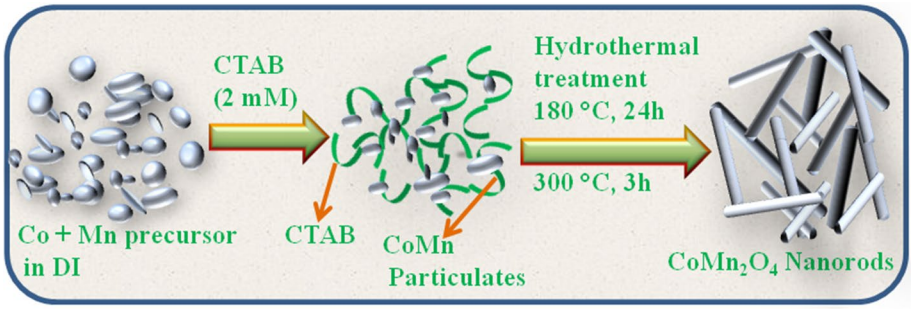

Fig.1 Schematic diagram for synthesis of $CoMn_2O_4$-4 material

X-ray diffraction studies as shown in Fig. 2. The intensities and positions of the peaks are more consistent with the standard diffraction pattern of the tetragonal, spinel $CoMn_2O_4$ phase with JCPDS card no.- 01-077-0471. The distinctive peaks located at 29.3, 30.8, 33.3, 36, 36.8, 44.2, 52.7, 56.5, 58.3, 65.6, and 71.2° are indexed to the (112), (200), (103), (211), (202), (220), (105), (303), (321), (116) and (305) planes, respectively. All diffraction peaks are appeared as same, however, intensities only vary.

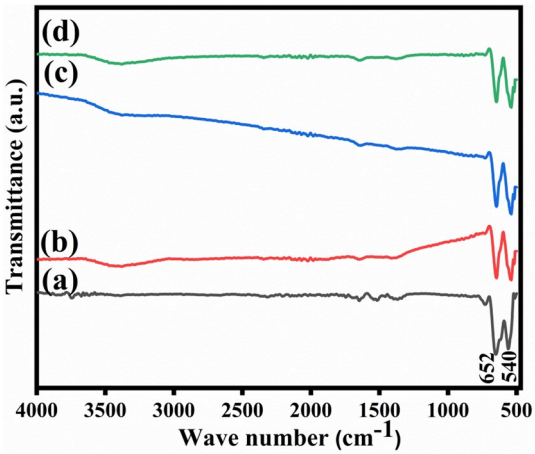

Fig. 3 FTIR spectra of $CoMn_2O_4$ materials. a $CoMn_2O_4$-1, (b) $CoMn_2O_4$-2, (c) $CoMn_2O_4$-3 and (d) $CoMn_2O_4$-4

FTIR spectroscopic analysis

The internal structure and bonding properties of the synthesized materials such as $CoMn_2O_4$-1, $CoMn_2O_4$-2, $CoMn_2O_4$-3 and $CoMn_2O_4$-4 were evaluated using FTIR spectroscopic analysis as shown in Fig. 3. It is worth to note that the impurity peaks do not visible in FTIR spectrum confirms the formation of pure $CoMn_2O_4$ materials. The FTIR spectrum provides two high-intensity peaks which are the characteristic peak of the spinel $CoMn_2O_4$ materials. The peaks appeared at 652 and 540 cm^{-1} are due to bending vibration of cobalt oxide at tetrahedral sites and manganese oxide at octahedral sites, respectively (Hosseini et al. 2011; Vigneshwaran et al. 2016). The basic characterization results such as XRD and FTIR have established the formation, crystalline phase and internal structure of the $CoMn_2O_4$ in the present CTAB assisted hydrothermals synthetic method.

Morphological analysis

The morphological features of $CoMn_2O_4$ were evaluated using FE-SEM analysis as shown in Figs. 4, 5. Figure 4 a, b shows the lower and higher magnification FESEM images of $CoMn_2O_4$-1 materials which shows irregular-shaped nanoparticles, which was synthesized without CTAB template. The definite-shaped nanoparticles with the size of 90 ± 5 nm are formed when introducing of 0.005 M of CTAB template ($CoMn_2O_4$-2) as shown in Fig. 4 c and d. When the CTAB concentration increased to 0.01 M ($CoMn_2O_4$-3), the same

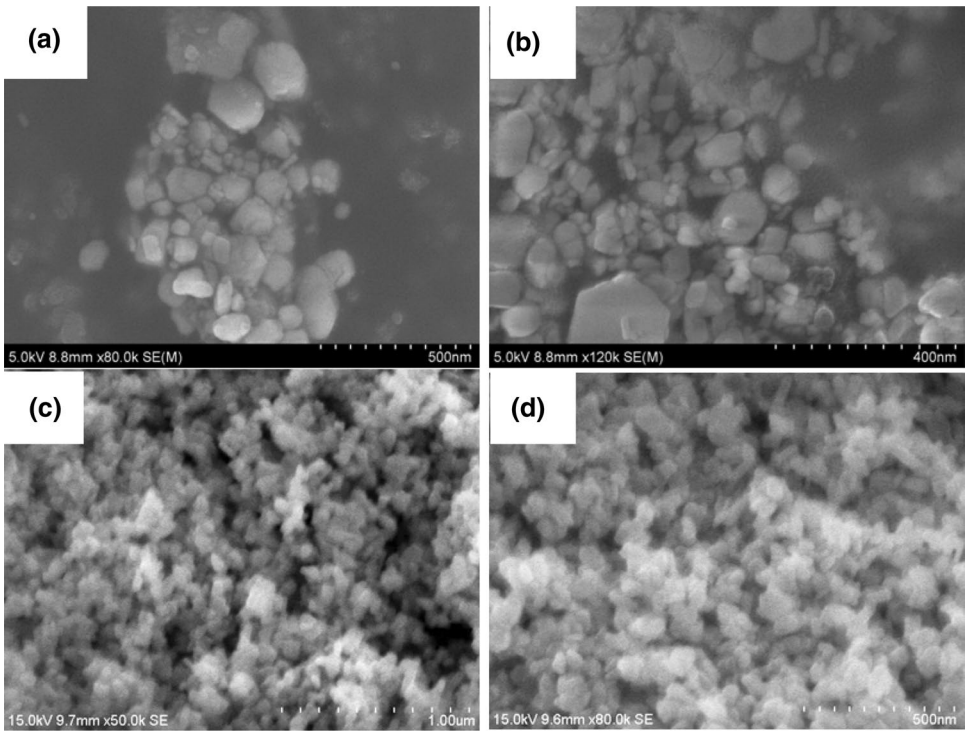

Fig. 4 Lower and higher magnification FESEM images of **a** and **b** $CoMn_2O_4$-1 and **c** and **d** $CoMn_2O_4$-2 materials

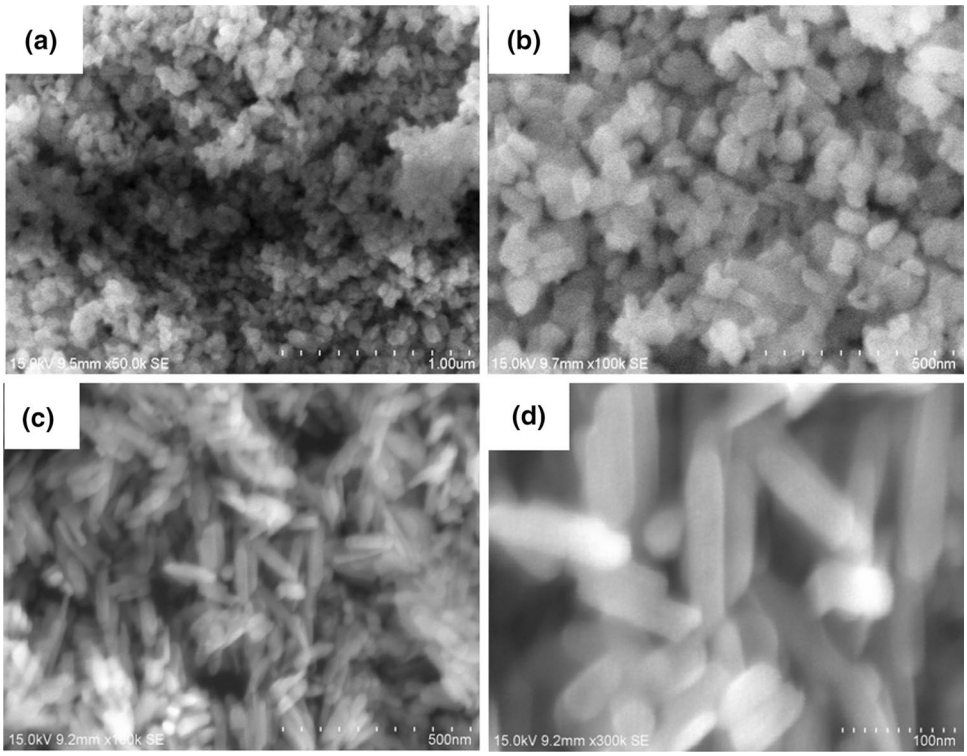

Fig. 5 Lower and higher magnification FESEM images of **a** and **b** $CoMn_2O_4$-3 and **c** and **d** $CoMn_2O_4$-4 materials

morphology was obtained and the shape of the nanoparticles are getting elongated which shows in Fig. 5a, b. Figure 5c, d shows the lower and higher magnification images of $CoMn_2O_4$-4 material which shows the edge-curved nanorod morphology.

The size and length of the nanorods are 30 ± 5 nm and 150 ± 5 nm, respectively. These results signify that the CTAB template has more consequences on the morphology of the $CoMn_2O_4$ materials. The nanorods morphology is more favored for electrochemical process since it provides high surface area for electrochemical redox reactions.

Electrochemical analysis

The supercapacitive features of the freshly prepared $CoMn_2O_4$ electrodes such as $CoMn_2O_4$-1, $CoMn_2O_4$-2, $CoMn_2O_4$-3 and $CoMn_2O_4$-4 were examined in a three electrode configuration using 2 M KOH electrolyte. Usually, the electrochemical properties can be demonstrated using different techniques including cyclic voltammetry (CV), chronopotentiometry (CP) and electrochemical impedance spectroscopy (EIS).

A cyclic voltammetric study is utilized to evaluate the redox behavior, capacitance and reversibility nature. Figure 6a–d shows the cyclic voltammetric curves of $CoMn_2O_4$-1, $CoMn_2O_4$-2, $CoMn_2O_4$-3 and $CoMn_2O_4$-4, respectively, which were demonstrated at the scan rates from 5 to 100 mV s^{-1} within a potential window from 0 to 0.5 V. All the CV curves exhibit the redox peaks such as the anodic peak located at approximately 0.31 V. whereas the cathodic peak positioned at approximately 0.22 V which is due to the redox process and signifying the pseudocapacitor behavior of the $CoMn_2O_4$ materials (Cai et al. 2014; Senthilkumar and Kalai Selvan 2014).

The redox reaction may be described in the following Eqs. 1, 2 and 3. (Yunyun et al. 2015)

$$CoMn_2O_2 + H_2O^- \rightarrow CoOOH + 2MnOOH + e^-, \quad (1)$$

$$MnOOH + OH^- \rightarrow MnO_2 + H_2O + e^- \quad (2)$$

$$CoOOH + OH^- \rightarrow H_2O + e^-. \quad (3)$$

The broadness of CV curves is increasing from $CoMn_2O_4$-1 to $CoMn_2O_4$-4 confirming the superior pseudocapacitance behavior of the $CoMn_2O_4$-4 material. The diffusive and capacitive contributions in CV analysis (for $CoMn_2O_4$-4 material) were calculated by using the Eq. (4).

$$I = av^b, \quad (4)$$

where I is the fitting current, v is the scan rate. The a and b are variables. The value of b is determined by plotting the log (i) versus log (v) curves as shown in Fig. 6e. The b value of 0.5 demonstrates diffusion controlled progression, whereas 1.0 indicates the surface capacitive controlled process. In the present investigation, the b

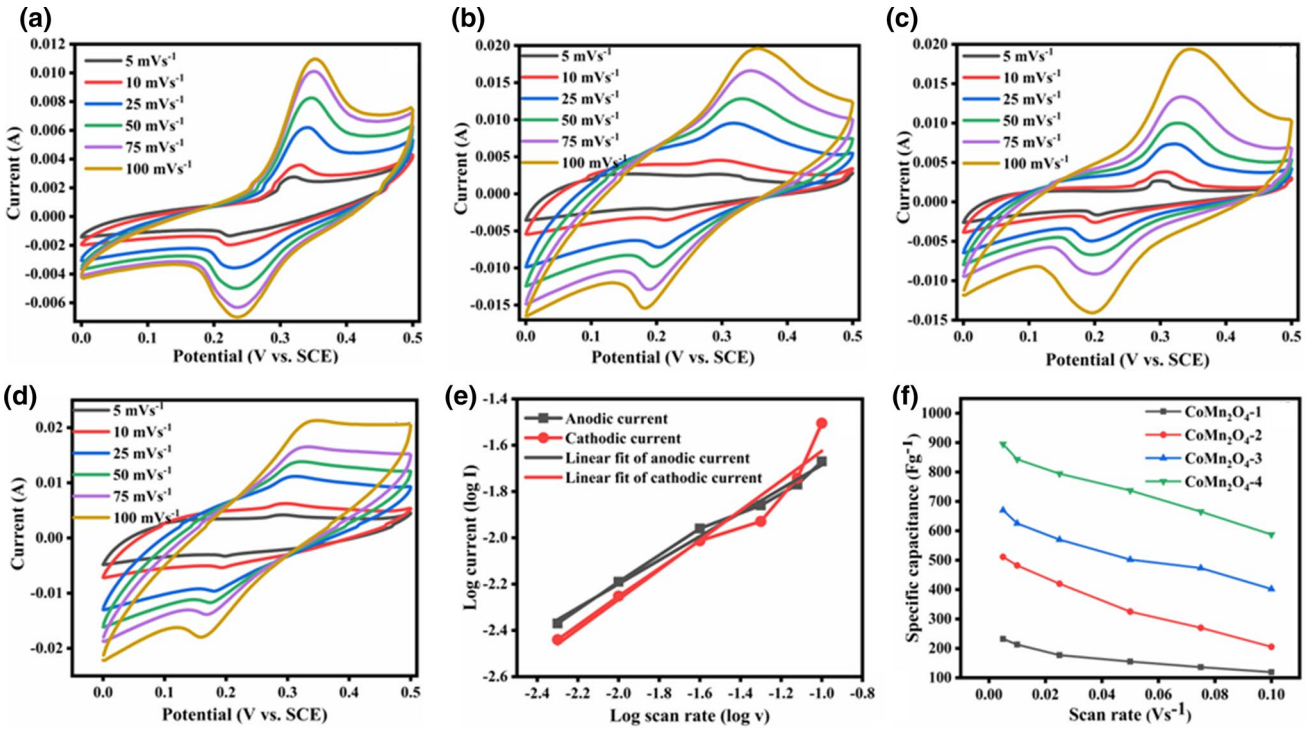

Fig. 6 CV curves of $CoMn_2O_4$ materials. **a** $CoMn_2O_4$-1, **b** $CoMn_2O_4$-2, **c** $CoMn_2O_4$-3 and **d** $CoMn_2O_4$-4, **e** plot of rate (log i vs. log v) for the redox peaks and **f** Scan rate vs specific capacitance graph

values are 0.64 and 0.72 for anodic and cathodic current, respectively. This indicates that the present energy storage process is mixed behavior of diffusive and capacitive controlled process. (Chen et al. 2019a, b; Zhang et al. 2020).

The quasi symmetric feature of the redox peaks and cycles attributes the outstanding reversibility of the $CoMn_2O_4$ electrodes. when the scan rate is raised from 5 to 100 mV s^{-1}, the current response enhance at the same time as the shape profile of the CV curves do not altered which suggesting enhanced mass transportation and rapid conduction of electrons in the electrode material during the electrochemical process(Jadhav et al. 2016). Interestingly, the peak appeared at the anodic current was shifted towards the positive region, whereas cathodic peak drift towards the more negative region which is due to ohmic resistance and electrical polarization behavior of $CoMn_2O_4$ electrodes(Cao et al. 2014). In addition, the area under the cyclic voltammetric curves is directly proportional to the specific capacitance of the corresponding electrodes. The $CoMn_2O_4$-4 provides higher area under the CV curves than other electrodes such as $CoMn_2O_4$-1, $CoMn_2O_4$-2 and $CoMn_2O_4$-3 confirming its superior pseudocapacitive behavior. The specific capacitance of the $CoMn_2O_4$ electrodes were calculated from the CV curves utilizing Eq. 5.

$$Csp = \frac{\int idV}{S.\Delta V.m}, \tag{5}$$

where $\int idV$ denotes the integral area of CV curve, ΔV potential limit (V), m mass of the active material (mg), and S the sweep rate (mV s^{-1}) from 5 to 100 mV s^{-1}. The obtained specific capacitance values are 232, 511, 670 and 895 Fg^{-1} for $CoMn_2O_4$-1, $CoMn_2O_4$-2, $CoMn_2O_4$-3 and $CoMn_2O_4$-4 electrodes, respectively, at a scan rate of 5 mV s^{-1}. The specific capacitance of $CoMn_2O_4$-4 electrode (895 Fg^{-1}) is approximately four-fold increases from the specific capacitance of the $CoMn_2O_4$-1electrode (232 Fg^{-1}). Additionally, the specific capacitance of the.

$CoMn_2O_4$-4 electrode is higher than previously published literatures based on Co_3O_4, (Co_3O_4 nanoparticles (519 Fg^{-1})(Vijayakumar et al. 2013), hollow Co_3O_4 nanowire (599 Fg^{-1}) (Xia et al. 2011) and Co_3O_4 nanowire (754 Fg^{-1}) (Tu et al. 2012) MnO_2 (MnO_2 nanostructure (311 Fg^{-1}) (Zhang et al. 2013), MnO_2 nanorods (649 Fg^{-1}) (Kumar et al. 2016) and α- MnO_2 nanorod (166.2 Fg^{-1}) (Li et al. 2011) and $CoMn_2O_4$ electrode materials ($CoMn_2O_4$ nanofibers (121 Fg^{-1}) (Alkhalaf et al. 2017), cubic $CoMn_2O_4$ particles (77.8 Fg^{-1}) (Chen et al. 2019a, b) and $CoMn_2O_4$ (700 Fg^{-1}) (Vigneshwaran et al. 2016). The superior

specific capacitance behavior of the $CoMn_2O_4$-4 electrode is explained as follows: (i) The one-dimensional nanorods exhibit high surface area which provides the more active sites for electrochemical reaction. (ii) The small dimensions of the nanorods not only enhance the transportation of electrolyte ions and also increase the absorption of ions during electrochemical analysis. (ii) It gives the short diffusion path for electron and ion transportations and remained their original structural natures.

The rate capabilities of all electrode materials were characterized through scan rate vs specific capacitance graph as shown in Fig. 6f. The specific capacitances decrease with the increasing of scan rate and this trend is explained as follows: at low scan rate, the larger time is allowed to perform electrochemical reaction actively in both inner and outer region of electrode materials and hence the specific capacitance increases. On the other hand, the outer region of electrode only participate in the electrochemical process during higher scan rate which is due to the shorter time and thus decrease the specific capacitance(Kim et al. 2016). The remaining characterizations such as electrochemical impedance spectroscopy, chronopotentiometry and cyclic stability studies were carried out only for $CoMn_2O_4$-4 electrode due to its better electrochemical properties.

The electrochemical impedance spectroscopic analyses were carried out to analyze intrinsic electrochemical properties of the $CoMn_2O_4$-4 electrode as shown in Fig. 7. Two main distinctive properties observed in the high- and low-frequency regions are ascribed to different resistance and capacitance phenomena during different interfacial processes in Faradaic reactions. The semicircle at high-frequency region is the characteristic of resistance at the solid oxide or electrode materials/liquid electrolyte interface owing to discontinuity in the charge transfer process. The straight line obvious at low-frequency region attributes the confirmation of diffusive charge transfer mechanism. The intercept of the real axis is due to internal resistances which are originated from the resistance produced from all the active electrode materials, the resistance of the electrolyte and the resistance created between material/current collector interfaces (contact resistance) (Bengoechea et al. 2002; Lu et al. 2016).

The more vertical line of the curve attributes the more facile electrolyte diffusion to the surface due to the small nanoparticle size and large surface area of the compared to the $CoMn_2O_4$ -4 sample(Xu et al. 2014a, b). Figure 8a shows the chronopotentiometric curves of the $CoMn_2O_4$-4 electrode at a current densities of 1, 2, 3, 4, 5, 10 and 20 Ag^{-1}. The potential limits from 0 to 0.45 V was chosen for chronopotentiometric analysis and it shown in Fig. 7. The non-linear behavior of the charge discharge curves confirms the pseudocapacitive nature which is more consistent with the CV analysis. It is interesting to note that there are two sections of CP curves, including the straight line and curved line which signifies the characteristic faradaic nature(Zhao et al. 2016). The specific capacitances were calculated by CP curves, using the Eq. 6.

$$Csp = \frac{I\Delta t}{m\Delta V}, \tag{6}$$

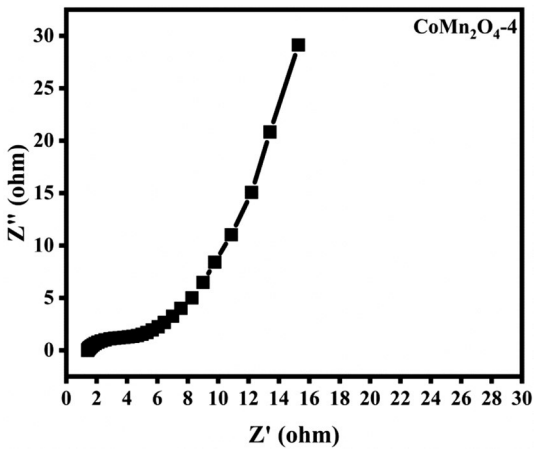

Fig. 7 Impedance spectra of $CoMn_2O_4$ materials

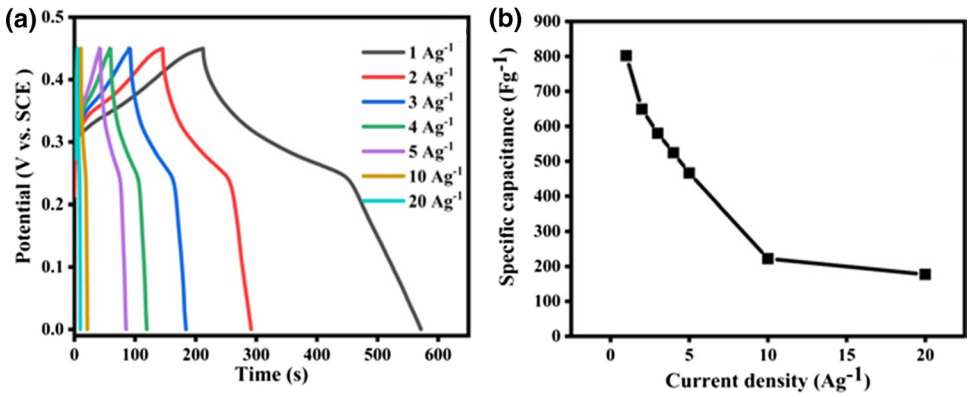

Fig. 8 **a** CP curves of $CoMn_2O_4$-4 material and **b** current density vs. Specific capacitance graph

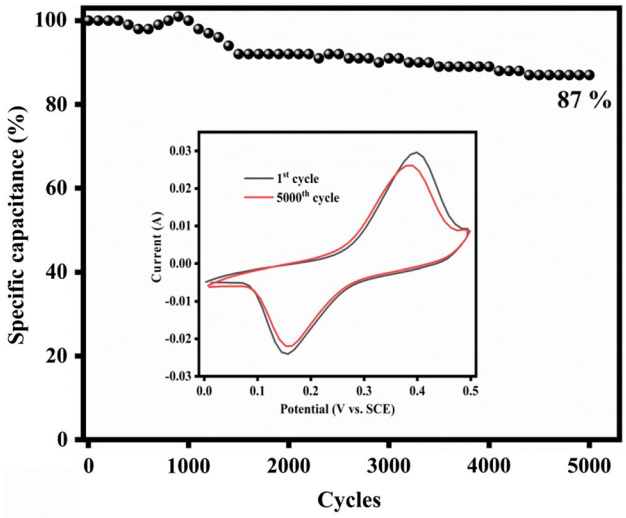

Fig. 9 Cyclic stability analysis of $CoMn_2O_4$-4 material at a scan rate of 100 mV s^{-1}

where I denotes discharge current density (A), Δt is the discharge time (s), ΔV the potential window (V) and m is the mass of the active material (mg). The $CoMn_2O_4$-4 electrode exhibit a specific capacitance of 802, 649, 580, 524, 466, 222 and 177Fg $^{-1}$ at a current densities of 1, 2, 3, 4, 5, 10 and 20 Ag^{-1}, respectively. The specific capacitance vs. current density graph is shown in Fig. 8b. The specific capacitance values decrease with increasing of current density which is due to the time limitation process and it is more reliable with the CV curves (Yesuraj et al. 2019).

Long-time cyclic stability behavior of the materials is also great importance for high performance supercapacitor application. Cyclic stability of $CoMn_2O_4$-4 electrode is further evaluated by using continuous 5000 CV cycles at high scan rate of 100 mVs^{-1} as shown in Fig. 9. The inset of Fig. 8 shows the 1st and 5000th cycles of cyclic stability studies. Initially, the amount of specific capacitance increases at 900th of cycles which is attributed to the rising of efficient interfacial area between the electrodes and electrolyte and along with the slow activation process of the $CoMn_2O_4$-4 electrode(Hou et al. 2016). After that, it gradually decreases and retained 87% of initial capacitance after 5000 cycles. The superior cyclic stability property is due to the nanorods structural features of $CoMn_2O_4$-4 electrode material. The superior specific capacitance and cyclic stability features implies probable application of $CoMn_2O_4$-4 nanorod in electrode material for supercapacitors.

Conclusion

The work established a simple CTAB assisted hydrothermal synthetic technique for the preparation of edge curved one-dimensional $CoMn_2O_4$ nanorods for pseudocapacitor electrode application followed by annealing process. In this process, the CTAB template plays a key role to control the morphological features of $CoMn_2O_4$ materials. The synthesized materials were characterized by XRD, FTIR and FESEM techniques to evaluate their formation, crystalline phase, bonding properties and structural features. The high concentration of CTAB provides edge curved one-dimensional nanorods structure. The electrochemical properties of the $CoMn_2O_4$ materials were evaluated using cyclic voltammetric, chronopotentiometric and electrochemical impedance spectroscopic analysis. The CV curves provide the specific capacitance of 895 Fg^{-1} at a scan rate of 5 mV s^{-1}, whereas CP curves provide the specific capacitance of 802 Fg^{-1} at a current density of 1 Ag^{-1}. Furthermore, $CoMn_2O_4$ electrode retained 87% of initial capacitance after 5000 CV cycles at a scan rate of 100 mV s^{-1}.The outstanding electrochemical features and superior cyclic stability facilitate the obtained $CoMn_2O_4$ material to be an important material for supercapacitor device applications.

Compliance with ethical standards

Conflict of interest On behalf of all the authors, the corresponding author states that there is no conflict of interest.

References

Abbasi L, Arvand M, Moosavifard SE (2020) Facile template-free synthesis of 3D hierarchical ravine-like interconnected $MnCo_2S_4$ nanosheet arrays for hybrid energy storage device. Carbon N Y 161:299–308. https://doi.org/10.1016/j.carbon.2020.01.094

Alkhalaf S, Ranaweera CK, Kahol PK et al (2017) Electrochemical energy storage performance of electrospun $CoMn_2O4$nanofibers. J Alloys Compd 692:59–66. https://doi.org/10.1016/j.jallcom.2016.09.005

Amiri M, Davarani SSH, Kaverlavani SK et al (2020) Construction of hierarchical nanoporous $CuCo_2V_2O_8$ hollow spheres as a novel electrode material for high-performance asymmetric supercapacitors. Appl Surf Sci 527:146855. https://doi.org/10.1016/j.apsusc.2020.146855

An C, Zhang Y, Guo H, Wang Y (2019) Metal oxide-based supercapacitors: progress and prospectives. Nanoscale Adv 1:4644–4658. https://doi.org/10.1039/c9na00543a

Bengoechea MR, Aliev FM, Pinto NJ (2002) Effects of confinement on the phase separation in emeraldine base polyaniline cast from 1-methyl-2-pyrrolidinone studied via dielectric spectroscopy. J Phys Condens Matter 14:11769–11778. https://doi.org/10.1088/0953-8984/14/45/318

Boisset A, Athouël L, Jacquemin J et al (2013) Comparative performances of birnessite and cryptomelane MnO_2 as electrode material in neutral aqueous lithium salt for supercapacitor application. J Phys Chem C 117:7408–7422. https://doi.org/10.1021/jp3118488

Cai D, Liu B, Wang D et al (2014) Facile hydrothermal synthesis of hierarchical ultrathin mesoporous $NiMoO_4$ nanosheets for high performance supercapacitors. Electrochim Acta 115:358–363. https://doi.org/10.1016/j.electacta.2013.10.154

Cao Y, Li W, Xu K et al (2014) $MnMoO_4{\cdot}4H_2O$ nanoplates grown on a Ni foam substrate for excellent electrochemical properties. J Mater Chem A 2:20723–20728. https://doi.org/10.1039/c4ta04019h

Che H, Liu A, Mu J et al (2016) Template-free synthesis of novel flower-like $MnCo_2O_4$ hollow microspheres for application in supercapacitors. Ceram Int 42:2416–2424. https://doi.org/10.1016/j.ceramint.2015.10.041

Chen LY, Kang JL, Hou Y et al (2013) High-energy-density nonaqueous MnO_2@nanoporous gold based supercapacitors. J Mater Chem A 1:9202–9207. https://doi.org/10.1039/c3ta11480e

Chen W, Rakhi RB, Hedhili MN, Alshareef HN (2014) Shape-controlled porous nanocarbons for high performance supercapacitors. J Mater Chem A 2:5236–5243. https://doi.org/10.1039/c3ta15245f

Chen F, Wang Z, Huo S et al (2019a) Cubic $CoMn_2O_4$ particles directly grown on Ni foam as binder-free electrode for asymmetric supercapacitors. Mater Lett 237:209–212. https://doi.org/10.1016/j.matlet.2018.11.100

Chen J, Yang B, Hou H et al (2019b) Disordered, large interlayer spacing, and oxygen-rich carbon nanosheets for potassium ion hybrid capacitor. Adv Energy Mater 9:1–9. https://doi.org/10.1002/aenm.201803894

Dhand C, Dwivedi N, Loh XJ et al (2015) Methods and strategies for the synthesis of diverse nanoparticles and their applications: a comprehensive overview. RSC Adv 5:105003–105037. https://doi.org/10.1039/c5ra19388e

Geng J, Ma C, Zhang D, Ning X (2020) Facile and fast synthesis of SnO_2 quantum dots for high performance solid-state asymmetric supercapacitor. J Alloys Compd 825:153850. https://doi.org/10.1016/j.jallcom.2020.153850

Hosseini SA, Salari D, Niaei A et al (2011) Chemical-physical properties of spinel $CoMn_2O_4$ nano-powders and catalytic activity in the 2-propanol and toluene combustion: effect of the preparation method. J Environ Sci Heal Part A Toxic/Hazardous Subst Environ Eng 46:291–297. https://doi.org/10.1080/10934529.2011.539093

Hou L, Bao R, Chen Z et al (2016) Comparative investigation of hollow mesoporous $NiCo_2S_4$ ellipsoids with enhanced pseudocapacitances towards high-performance asymmetric supercapacitors. Electrochim Acta 214:76–84. https://doi.org/10.1016/j.electacta.2016.08.038

Hu CC, Chang KH, Lin MC, Wu YT (2006) Design and tailoring of the nanotubular arrayed architecture of hydrous RuO_2 for next generation supercapacitors. Nano Lett 6:2690–2695. https://doi.org/10.1021/nl061576a

Jadhav HS, Pawar SM, Jadhav AH et al (2016) Hierarchical mesoporous 3D Flower-like $CuCo_2O_4$/NF for high-performance electrochemical energy storage. Sci Rep 6:2–13. https://doi.org/10.1038/srep31120

Kim T, Ramadoss A, Saravanakumar B et al (2016) Applied surface science synthesis and characterization of $NiCo_2O_4$ nanoplates as efficient electrode materials for electrochemical supercapacitors. Appl Surf Sci 370:452–458. https://doi.org/10.1016/j.apsusc.2016.02.147

Kumar A, Sanger A, Kumar A et al (2016) Sputtered synthesis of MnO_2nanorods as binder free electrode for high performance symmetric supercapacitors. Electrochim Acta 222:1761–1769. https://doi.org/10.1016/j.electacta.2016.10.161

Li Y, Xie H, Wang J, Chen L (2011) Preparation and electrochemical performances of α-MnO_2 nanorod for supercapacitor. Mater Lett 65:403–405. https://doi.org/10.1016/j.matlet.2010.10.048

Li X, Li X, Wang G et al (2013) Flexible supercapacitor based on MnO_2 nanoparticles via electrospinning. J Mater Chem A 1:10103–10106. https://doi.org/10.1039/c3ta11727h

Li Y, Han X, Yi T et al (2019) Review and prospect of $NiCo_2O_4$ -based composite materials for supercapacitor electrodes. J Energy Chem. https://doi.org/10.1016/j.jechem.2018.05.010

Low WH, Khiew PS, Lim SS et al (2019) Recent development of mixed transition metal oxide and graphene/mixed transition metal oxide based hybrid nanostructures for advanced supercapacitors. J Alloys Compd 775:1324–1356. https://doi.org/10.1016/j.jallcom.2018.10.102

Lu Y, Zhang Z, Liu X et al (2016) $NiCo_2S_4$/carbon nanotube nanocomposites with a chain-like architecture for enhanced supercapacitor performance. CrystEngComm 18:7696–7706. https://doi.org/10.1039/c6ce01556e

Makino S, Yamauchi Y, Sugimoto W (2013) Synthesis of electrodeposited ordered mesoporous RuOx using lyotropic liquid crystal and application toward micro-supercapacitors. J Power Sources 227:153–160. https://doi.org/10.1016/j.jpowsour.2012.11.032

Mary AJC, Bose AC (2018) Surfactant assisted $ZnCo_2O_4$ nanomaterial for supercapacitor application. Appl Surf Sci 449:105–112. https://doi.org/10.1016/j.apsusc.2018.01.117

Moosavifard SE, Saleki F, Mohammadi A et al (2020) Construction of hierarchical nanoporous bimetallic copper-cobalt selenide hollow spheres for hybrid supercapacitor. J Electroanal Chem. https://doi.org/10.1016/j.jelechem.2020.114295

Naeem F, Naeem S, Zhao Z et al (2020) Atomic layer deposition synthesized ZnO nanomembranes: A facile route towards stable supercapacitor electrode for high capacitance. J Power Sources 451:227740. https://doi.org/10.1016/j.jpowsour.2020.227740

Paquin F, Rivnay J, Salleo A et al (2015) Multi-phase semicrystalline microstructures drive exciton dissociation in neat plastic semiconductors. J Mater Chem C 3:10715–10722. https://doi.org/10.1039/b000000x

Pu J, Wang J, Jin X et al (2013) Porous hexagonal $NiCo_2O_4$ nanoplates as electrode materials for supercapacitors. Electrochim Acta 106:226–234. https://doi.org/10.1016/j.electacta.2013.05.092

Senthilkumar B, KalaiSelvan R (2014) Hydrothermal synthesis and electrochemical performances of 1.7V NiMoO4. xH2O||FeMoO4 aqueous hybrid supercapacitor. J Colloid Interface Sci 426:280–286. https://doi.org/10.1016/j.jcis.2014.04.010

Simon P (2008) Simon 2009. Nat Mater 7:845–854

Tu J, Gu C, Zhao X et al (2012) Freestanding Co_3O_4 nanowire array for high performance supercapacitors. RSC Adv 2:1835. https://doi.org/10.1039/c1ra00771h

Vigneshwaran P, Kandiban M, Senthil Kumar N et al (2016) A study on the synthesis and characterization of $CoMn_2O_4$ electrode material for supercapacitor applications. J Mater Sci Mater Electron 27:4653–4658. https://doi.org/10.1007/s10854-016-4343-6

Vijayakumar S, Kiruthika Ponnalagi A, Nagamuthu S, Muralidharan G (2013) Microwave assisted synthesis of Co_3O_4 nanoparticles for high-performance supercapacitors. Electrochim Acta 106:500–505. https://doi.org/10.1016/j.electacta.2013.05.121

Vijayakumar S, Nagamuthu S, Ryu KS (2017) $CuCo_2O_4$ flowers/Ni-foam architecture as a battery type positive electrode for high performance hybrid supercapacitor applications. Electrochim Acta 238:99–106. https://doi.org/10.1016/j.electacta.2017.03.178

Wang Y, Shen C, Niu L et al (2016) Hydrothermal synthesis of $CuCo_2O_4$/CuO nanowire arrays and RGO/Fe_2O_3 composites for high-performance aqueous asymmetric supercapacitors. J Mater Chem A 4:9977–9985. https://doi.org/10.1039/c6ta02950g

Wu Z, Zhu Y, Ji X (2014) $NiCo_2O_4$ -based materials for electrochemical supercapacitors. J Mater Chem A 2:14759–14772. https://doi.org/10.1039/c4ta02390k

Wulan Septiani NL, Kaneti YV, Fathoni KB et al (2020) Self-assembly of nickel phosphate-based nanotubes into two-dimensional crumpled sheet-like architectures for high-performance asymmetric supercapacitors. Nano Energy 67:104270. https://doi.org/10.1016/j.nanoen.2019.104270

Xia XH, Tu JP, Mai YJ et al (2011) Self-supported hydrothermal synthesized hollow $Co3O_4$ nanowire arrays with high supercapacitor capacitance. J Mater Chem 21:9319–9325. https://doi.org/10.1039/c1jm10946d

Xu K, Li W, Liu Q et al (2014a) Hierarchical mesoporous $NiCo_2O_4$@MnO_2 core-shell nanowire arrays on nickel foam for aqueous asymmetric supercapacitors. J Mater Chem A 2:4795–4802. https://doi.org/10.1039/c3ta14647b

Xu Y, Wang X, An C, Wang Y, Jiaoa L, Yuana H (2014b) Facile synthesis route of porous $MnCo_2O_4$ and $CoMn_2O_4$ nanowires and their excellent electrochemical properties in supercapacitor. J Mater Chem A 20:16480–16488. https://doi.org/10.1039/C4TA03123G

Yan X, Tong X, Wang J et al (2014) Synthesis of mesoporous NiO nanoflake array and its enhanced electrochemical performance for supercapacitor application. J Alloys Compd 593:184–189. https://doi.org/10.1016/j.jallcom.2014.01.036

Yang J, Lan T, Liu J et al (2013) Supercapacitor electrode of hollow spherical V_2O_5 with a high pseudocapacitance in aqueous solution. Electrochim Acta 105:489–495. https://doi.org/10.1016/j.electacta.2013.05.023

Yesuraj J, Samuel AS, Elaiyappillai E et al (2017) A facile sonochemical assisted synthesis of α-$MnMoO_4$/PANI nanocomposite electrode for supercapacitor applications. J Electroanal Chem 797:78–88. https://doi.org/10.1016/j.jelechem.2017.05.019

Yesuraj J, Suthanthiraraj SA, Padmaraj O (2019) Materials science in semiconductor processing synthesis, characterization and electrochemical performance of DNA- templated Bi2MoO6 nanoplates for supercapacitor applications. Mater Sci Semicond Process 90:225–235. https://doi.org/10.1016/j.mssp.2018.10.030

Yunyun F, Xu L, Wankun Z et al (2015) Spinel $CoMn_2O_4$ nanosheet arrays grown on nickel foam for high-performance supercapacitor electrode. Appl Surf Sci 357:2013–2021. https://doi.org/10.1016/j.apsusc.2015.09.176

Zhang X, Sun X, Zhang H et al (2013) Microwave-assisted reflux rapid synthesis of MnO_2 nanostructures and their application in supercapacitors. Electrochim Acta 87:637–644. https://doi.org/10.1016/j.electacta.2012.10.022

Zhang C, Huang Y, Tang S et al (2017) High-energy all-solid-state symmetric supercapacitor based on Ni_3S_2 mesoporous nanosheet-decorated three-dimensional reduced graphene oxide. ACS Energy Lett 2:759–768. https://doi.org/10.1021/acsenergylett.7b00078

Zhang C, Zheng B, Huang C et al (2019) Heterostructural three-dimensional reduced graphene oxide/$CoMn_2O_4$ nanosheets toward a wide-potential window for high-performance supercapacitors. ACS Appl Energy Mater 2:5219–5230. https://doi.org/10.1021/acsaem.9b00904

Zhang C, Peng Z, Chen Y et al (2020) Efficient coupling of semiconductors into metallic MnO_2@$CoMn_2O_4$ heterostructured electrode with boosted charge transfer for high-performance supercapacitors. Electrochim Acta 347:136246. https://doi.org/10.1016/j.electacta.2020.136246

Zhao G, Zhang N, Sun K (2013) Porous MoO_3 films with ultra-short relaxation time used for supercapacitors. Mater Res Bull 48:1328–1332. https://doi.org/10.1016/j.materresbull.2012.11.080

Zhao C, Ju P, Wang S et al (2016) One-step hydrothermal preparation of TiO_2/RGO/$Ni(OH)_2$/NF electrode with high performance for supercapacitors. Electrochim Acta 218:216–227. https://doi.org/10.1016/j.electacta.2016.09.122

Zhu M, Weber CJ, Yang Y et al (2008) Chemical and electrochemical ageing of carbon materials used in supercapacitor electrodes. Carbon N Y 46:1829–1840. https://doi.org/10.1016/j.carbon.2008.07.025

Zhu L, Chang Z, Wang Y et al (2015) Core-shell MnO_2@Fe_2O_3 nanospindles as a positive electrode for aqueous supercapacitors. J Mater Chem A 3:22066–22072. https://doi.org/10.1039/c5ta05556c